NASA TECHNICAL MEMORANDUM

NASA TM X-71571

NASA TM X-71571

EMISSION CALIBRATION OF A J-58 AFTERBURNING TURBOJET ENGINE AT SIMULATED SUPERSONIC, STRATOSPHERIC FLIGHT CONDITIONS

by James D. Holdeman
Lewis Research Center
Cleveland, Ohio 44135

TECHNICAL PAPER proposed for presentation at Second International Conference on the Environmental Impact of Aerospace Operations in the High Atmosphere sponsored by the American Meteorological Society and the American Institute of Aeronautics and Astronautics
San Diego, California, July 8-10, 1974

EMISSION CALIBRATION OF A J-58 AFTERBURNING TURBOJET ENGINE AT SIMULATED SUPERSONIC, STRATOSPHERIC FLIGHT CONDITIONS

James D. Holdeman

NASA-Lewis Research Center
Cleveland, Ohio

E-7935

ABSTRACT

Emissions of total oxides of nitrogen, unburned hydrocarbons, and carbon monoxide from a J-58 engine at simulated flight conditions of Mach 2.0, 2.4, and 2.8 at 19.8 km altitude are reported. For each flight condition, measurements were made for four engine power levels from maximum power without afterburning through maximum afterburning. These measurements were made 7 cm downstream of the engine primary nozzle using a single point traversing gas sample probe. Results show that emissions vary with flight speed, engine power level, and with radial position across the exhaust.

1. INTRODUCTION

Testing of a J-58 afterburning turbojet engine was conducted to determine its emissions of oxides of nitrogen, unburned hydrocarbons, carbon monoxide, and carbon dioxide, at simulated supersonic, high altitude flight conditions. Emission measurements from aircraft turbine engines, and in particular, afterburning engines, at high altitude supersonic flight conditions are relevant to answering questions about the environmental impact of the supersonic transport. Previous studies dealing with aircraft jet engine emissions at altitude conditions are reported by Diehl (1971, 1973), Palcza (1971), Davidson and Domal (1973), German et. al. (1973), and Diehl and Blaglow (1974). In these, various engines and flight conditions have been examined. Detailed profiles of local fuel-air ratio, total temperature, the oxides of nitrogen, unburned hydrocarbons, and carbon monoxide at the exhaust of a J-58 engine appear in a previous NASA report (Holdeman; 1974). Included there also are emission index profiles for the oxides of nitrogen, unburned hydrocarbons, carbon monoxide, and carbon dioxide. Detailed information of this type is essential as initial conditions to studies of chemical kinetics in the near wake of a supersonic aircraft. However, if the chemical composition of the exhaust does not change substantially in the first few diameters downstream of the exhaust plane, then the integrated average emissions are sufficient as initial conditions for assessing the dispersion and dilution of the exhaust.

The purpose of the present investigation is to provide an emissions calibration for the J-58 engine for subsequent use in the NASA Stratospheric Jet Wake Experiment (Farlow et. al.; 1974). In this program, in-flight sampling of exhaust constituents will be made in the wake of a YF-12 aircraft, powered by two J-58 engines, during supersonic, stratospheric flight. The emissions calibration tests will provide the initial conditions for assessing the dispersion and dilution of exhaust products in the stratosphere. In addition, these tests will add to the general knowledge about emissions from afterburning turbojet engines at high altitude conditions. Although emission levels for the J-58 engine may not necessarily be representative of emissions from engines designed for present or future commercial supersonic aircraft, the trends should be similar.

In this paper, the integrated average emissions (not previously published) and selected profile data are presented to show the variations in exhaust parameters which occur as a function of flight speed and power level. The present investigation was conducted in the Propulsion Systems Laboratory at the Lewis Research Center. Test conditions included simulated flight speeds of Mach 2.0, 2.4, and 2.8, all at 19.8 km altitude. At each flight condition, data traverses across the diameter of the primary exhaust nozzle were made for four engine power levels from maximum power without afterburning to maximum afterburning.

2. APPARATUS

The J-58 engine is an afterburning turbojet designed for operation at flight speeds in excess of Mach 2 at stratospheric altitudes. The engine was tested in the Propulsion Systems Laboratory at the Lewis Research Center. This altitude chamber facility and associated air handling equipment provided conditioned inlet airflow and appropriate exhaust pressure to accurately simulate the conditions at the engine inlet and exhaust corresponding to the selected supersonic flight conditions. The engine operates using JP-7 fuel. This fuel was heated to 395 K prior to entering the engine to simulate the condition on board the aircraft during supersonic flight.

A single point, traversing, water-cooled gas sample probe was used to obtain emission measurements. The probe and its traversing mechanism are shown mounted behind the engine in figure 1(a). The traversing mechanism had the capability to translate the probe ± 60 cm horizontally and ± 20 cm vertically from the engine centerline.

The sensor area of the probe is shown in figure 1(b). A total pressure sensor was mounted 2.5 cm above the sample probe and three unshielded iridium/iridium-rhodium thermocouples were mounted 2.5 and 5 cm below and 5 cm above the gas sample probe. The gas sample sensor had an i.d. of 0.717 cm. The probe tip extended 1.9 cm forward of the rake body. This section was

water-cooled for a distance of 8 cm downstream from the tip both for sample conditioning and probe integrity. Following this section, the sample line increased to 0.818 cm i.d. (3/8 in. o.d.). For afterburning conditions, a second water-cooled heat exchanger on the next 30 cm of line was used to provide additional quenching of the sample. Approximately 10 meters of 0.95 cm stainless-steel line was used to transport the sample to the analyzers. In order to prevent condensation of water and to minimize adsorbtion-desorbtion effects of hydrocarbon compounds, the line was heated with steam at 428 K. Four heated metal bellows pumps (two pumps in series in each of two parallel legs) were used to supply sufficient gas sample pressure, 17 N/cm^2, to operate the analytical instruments. The gas sample line residence time was less than 2 seconds for all test conditions.

The exhaust gas analysis system is a packaged unit consisting of four commercially available instruments along with associated peripheral equipment necessary for sample conditioning and instrument calibration. The hydrocarbon content of the exhaust gas was measured on a wet basis using a Beckman Instruments Model 402 Hydrocarbon Analyzer. This instrument is of the flame ionization detector type. The concentration of the oxides of nitrogen was measured on a dry basis using a Thermo Electron Corporation Model 10A Chemiluminescence Analyzer. This instrument includes a thermal converter to reduce NO_2 to NO. Data were obtained as total NO_x ($NO + NO_2$). Both carbon monoxide and carbon dioxide were measured dry using analyzers of the nondispersive infrared (NDIR) type. These instruments were Beckman Instruments Model 315B.

3. TEST CONDITIONS AND PROCEDURE

The engine test conditions are presented in table I. Engine inlet air was conditioned to correspond to the values at the engine face for supersonic flight speeds of Mach 2.0, 2.4, and 2.8 at an altitude of 19.8 kilometers. For each flight condition, tests were made at four engine power settings from military through maximum afterburning, see table I. The altitude chamber pressure for each flight condition was selected to ensure a hard choke at the engine primary exhaust nozzle. Note that the altitude chamber pressure does not need to be equal to the ambient static pressure for the simulated altitude. The internal performance of the engine is correctly simulated for all pressures low enough to choke the nozzle.

Emission traverses were made at the plane of the primary nozzle (actually the probe was 6.7 cm from the exit plane when the engine was cold with the nozzle wide open). Data were obtained at 5 cm (nominal) intervals across the horizontal exhaust diameter resulting in approximately 20 data points per traverse. These small increments were necessary to document the steep gradients in emissions and temperature found in afterburning operation. The interval was increased to nominally 7.5 cm for military power tests since emissions and temperature gradients at this condition were much less than for afterburning conditions. The time required for each traverse varied from 30 to 45 minutes. All gas analysis instruments were checked for zero and span prior to each traverse. Complete surveys at each flight condition (four power levels) required approximately four hours of continuous engine operation.

Concentrations which were measured on a dry basis (NO_x, CO, and CO_2) are reported on a wet basis, correcting for water vapor, including both inlet air humidity and water vapor from combustion. Emission levels of all constituents were converted to emission index (EI) parameters based on the local (gas sample) fuel-air ratio according to the relations given in ARP 1256 (Anon.; 1971). Integrated average emission indices were obtained by integrating the local emission index values across the exhaust diameter. Average concentrations were calculated from the integrated average emission index and the integrated average fuel-air ratio.

4. RESULTS AND DISCUSSION

Results from the emissions and temperature measurements are discussed in the following paragraphs. All data shown were obtained in traversing the horizontal diameter of the exhaust. At the Mach 2.0 condition limited data were obtained up to 20 cm above and below the engine centerline on the vertical diameter. These data showed variations similar to those on the horizontal diameter.

4.1 Fuel-air Ratio and Exhaust Temperature

The local fuel-air ratio profiles calculated from the gas sample measurements are shown in figure 2. The horizontal axis on the figures is the radial distance from the engine centerline nondimensionalized by the calculated exit radius (R_8) at each condition. This radius varies with flight condition and engine power level. Data for the Mach 2.0 flight condition is shown in part (a) of the figure, data for Mach 2.4 is shown in part (b), and data for Mach 2.8 is shown in part (c). In all cases the simulated flight altitude is 19.8 kilometers.

For each flight condition, data are shown for four engine power levels; military (maximum power without afterburning), minimum afterburning (Min A/B), an intermediate afterburning power level (Int A/B), and maximum afterburning (Max A/B), see table I. The integrated average fuel-air ratios obtained from the profiles are listed adjacent to the symbol designations. For all conditions, the measured overall (table I) and integrated average values (figure 2) differ by less than 8 percent.

The integrated average exhaust temperatures are given in table I for the several power levels at each flight condition. The variations in temperature across the exhaust diameter follow the same trends as seen in the fuel-air ratio profiles. At military power, the temperature is very uniform across the exhaust, however, in afterburning modes significant temperature gradients exist.

For minimum and intermediate afterburning

conditions, temperatures in the region downstream of the flame holders were typically 10 percent above the average, with temperatures near the engine centerline typically 20 percent less than the average. At maximum afterburning, temperatures across the diameter were typically within ±6 percent of the average. No radiation correction was applied to the measured temperatures.

4.2 Oxides of Nitrogen Emissions

The volumetric exhaust concentration profiles of the oxides of nitrogen for each of the conditions are shown in figure 3. The average concentrations are listed in the key for each condition. NO_x concentrations at military power are nearly uniform across the exhaust. In afterburning modes, significant gradients in NO_x are observed across the exhaust for all conditions. The values shown are total NO_x ($NO + NO_2$) for all conditions except maximum afterburning at Mach 2.4. At this condition the converter on the chemiluminescence instrument was inadvertently turned off, thus the values shown represent NO only for this condition.

For all conditions except maximum afterburning at Mach 2.8, the measured NO_x on the engine centerline is less in afterburning than at the corresponding military power level. For all conditions the NO_x concentration at mid-radius (downstream of the afterburner flame holders) is greater than that at the same radius at military power.

The variation of the integrated average NO_x emission indices with flight speed is shown on figure 4. At military power the NO_x emission indices show a nearly linear increase from Mach 2.0 to Mach 2.8. NO_x emission indices in afterburning are approximately 45 percent of the value at military power for each flight condition, with only a very slight decrease indicated with increasing power in afterburning. The substantial decrease in the NO_x emission index in going from military to afterburning operation indicates that the large increase in fuel-air ratio is not accompanied by a corresponding increase in NO_x concentration; see figures 2 and 3.

4.3 Unburned Hydrocarbon Emissions

Exhaust concentrations of unburned hydrocarbons, as ppm C (parts per million carbon by volume), are shown in figure 5(a), (b), and (c) for Mach 2.0, 2.4, and 2.8, respectively. Average concentrations are given in the key. At military power, unburned hydrocarbons were uniform across the diameter and were less than 10 ppm C, corresponding to emission indices of less than 0.3 for all flight conditions. To avoid congestion, these values are not shown on the figure.

For minimum afterburning, unburned hydrocarbon concentrations on the order of 10,000 ppm C were observed on the engine centerline at all flight conditions. However, the hydrocarbon concentrations at radii greater than $R_8/2$ were at least two orders of magnitude less than the centerline value.

For the Mach 2.0 condition, high centerline hydrocarbon concentrations were observed for all afterburner power levels, but the width of the zone decreased with increasing power. For both Mach 2.4 and 2.8, the centerline concentration and the radial extent of the zone of high hydrocarbons decreased with increasing power. For maximum afterburning at Mach 2.8, the concentration of unburned hydrocarbons did not exceed 10 ppm C anywhere across the diameter; these low concentrations are not shown on figure 5(c).

The integrated average HC emission indices are shown in figure 6. Values for all power levels decrease with increasing flight speed, as a result of increasing pressure and temperature which increases combustion efficiency. At military power, unburned hydrocarbon emission indices are very low for all flight speeds.

In afterburning modes, the integrated average emission indices are high where high concentrations were measured in the center region of the exhaust. However, the local emission indices at radii greater than R/R_8=.5 are of the same order of magnitude as the emission index at the corresponding military power level.

4.4 Carbon Monoxide Emissions

Carbon monoxide concentration profiles are shown in figure 7 for each of the conditions tested. Average concentrations are given in the key. At military power, the CO emissions are low and uniform across the exhaust; to avoid congestion on the figure these are not shown. In afterburning modes, CO emissions are substantially higher than at military power for all flight speeds. The regions of the exhaust in which CO emissions are highest appear to be very dependent on afterburning power level. At minimum and intermediate afterburning CO emissions are high in the center region where unburned hydrocarbon emissions are also high. At intermediate afterburning, the CO concentrations at larger radii (R/R_8 > 0.5) are slightly greater than at minimum afterburning.

At maximum afterburning, CO emissions are high at radii near R/R_8 = 0.7. This is not unexpected since the local fuel-air ratio (fig. 2) is near stoichiometric at this radius, and the equilibrium CO concentration would be on the order of 2 percent. For Mach 2.0, the CO is also high in the center region, but for Mach 2.4 the center region CO is less than at larger radii, and at Mach 2.8, CO is very low in the center.

The integrated average emission indices for carbon monoxide are shown in figure 8. As with the unburned hydrocarbons, CO decreases with increasing flight speed for all power levels. However, for carbon monoxide, the highest integrated emission index values occur at maximum afterburning. This is a direct consequence of the near-equilibrium CO levels at radii where the local fuel-air ratio is near or above stoichiometric, and thus does not represent inefficiency. At minimum afterburning, the integrated CO emission index values are high for all flight speeds,

indicating that at this power level, combustion is incomplete at the sampling station for all speeds.

5. SUMMARY OF RESULTS

Gaseous emissions from a J-58 afterburning turbojet engine were measured at simulated flight conditions of Mach 2.0, 2.4, and 2.8 at 19.8 km altitude. For each flight condition, detailed profile measurements were made for four engine power levels from military through maximum afterburning. These measurements were made on a single diameter at the engine primary nozzle using a single point traversing gas sample probe.

The principal results of this investigation are given below:

a. In afterburning modes there are significant gradients in exhaust temperature, local fuel air ratio, and species concentrations across the exhaust plane. It was found that traverse increments on the order of 0.1 of the exhaust radius were required to document these gradients.

b. Oxides of nitrogen emissions increase by slightly more than a factor of two from Mach 2.0 to 2.8. The NO_x emission index values for military power at Mach 2.0, 2.4, and 2.8 indicate that the increase is nearly linear with increasing Mach number in this range.

c. For each flight condition the NO_x emission indices in afterburning modes are approximately 45 percent of the value at military power for the same flight speed.

d. At military power, unburned hydrocarbon emission indices were less than 0.3 for all flight speeds.

e. In afterburning modes, hydrocarbon emissions were substantially higher than at military power due to high hydrocarbon concentrations in the center region of the exhaust. The peak concentrations and the radial extent of this region decreased with increasing flight speed and increasing power level.

f. The carbon monoxide emission index at military power for Mach 2.0 was approximately 2.5 g CO/kg fuel and decreased with increasing flight speed.

g. In afterburning modes, CO emissions were substantially higher than at military power for all flight speeds. The CO levels, and the regions of the exhaust in which these emissions are highest is very dependent on afterburning power level as well as flight speed.

REFERENCES

Anon., 1971: Procedure for the Continuous Sampling and Measurement of Gaseous Emissions from Aircraft Turbine Engines. Aerospace Recommended Practice 1256, SAE.

Davidson, D. L., and A. F. Domal, 1973: Emission Measurements of a J93 Turbojet Engine. ARO-ETF-TR-73-46, ARO Inc. (AD-766648; AEDC-TR-73-132; FAA-RD-73-66).

Diehl, L. A., 1971: Preliminary Investigation of Gaseous Emissions from Jet Engine Afterburners. NASA TM X-2323.

____, 1973: Measurement of Gaseous Emissions from an Afterburning Turbojet Engine at Simulated Altitude Conditions. NASA TM X-2726.

____, and J. A. Biaglow, 1974: Measurement of Gaseous Emissions from a Turbofan Engine at Simulated Altitude Conditions. NASA TM X-3046.

Farlow, N. H., V. R. Watson, H. Hoshizaki, R. J. Conti, and J. W. Meyer, 1974: Measurements of Supersonic Jet Aircraft Wakes in the Stratosphere. AMS/AIAA Second International Conference on the Environmental Impact of Aerospace Operations in the High Atmosphere, San Diego, California; July 8-10, 1974.

German, R. C., M. D. High, and C. E. Robinson, 1973: Measurement of Exhaust Emissions from a J85-GE-5B Engine at Simulated High-Altitude Supersonic Free-Stream Flight Conditions. ARO-PWT-TR-73-49, ARO Inc. (AD-764-717; AEDC-TR-73-103; FAA-RD-73-92).

Holdeman, J. D., 1974: Gaseous Exhaust Emissions from a J-58 Engine at Simulated Supersonic Flight Conditions. NASA TM X-71532.

Palcza, J. L., 1971: Study of Altitude and Mach Number Effects on Exhaust Gas Emissions of an Afterburning Turbofan Engine. NAPTC-ATD-212, Naval Air Propulsion Test Center (AD-741249; FAA-RD-72-31).

TABLE I. - TEST CONDITIONS

[Simulated altitude = 19.8 km]

	Mach number		
	2.0	2.4	2.8
Engine inlet temperature, K	390	465	553
Engine inlet pressure, atm	0.42	0.75	1.35
Altitude chamber pressure, atm	0.22	0.30	0.42
Overall fuel-air ratio, f/a			
Military	0.018	0.015	0.013
Min A/B	0.042	0.037	0.033
Int A/B	0.050	0.044	0.040
Max A/B	0.064	0.059	0.057
Average exhaust temperature, K			
Military	993	989	988
Min A/B	1612	1628	1592
Int A/B	1785	1821	1769
Max A/B	1954	2011	2062

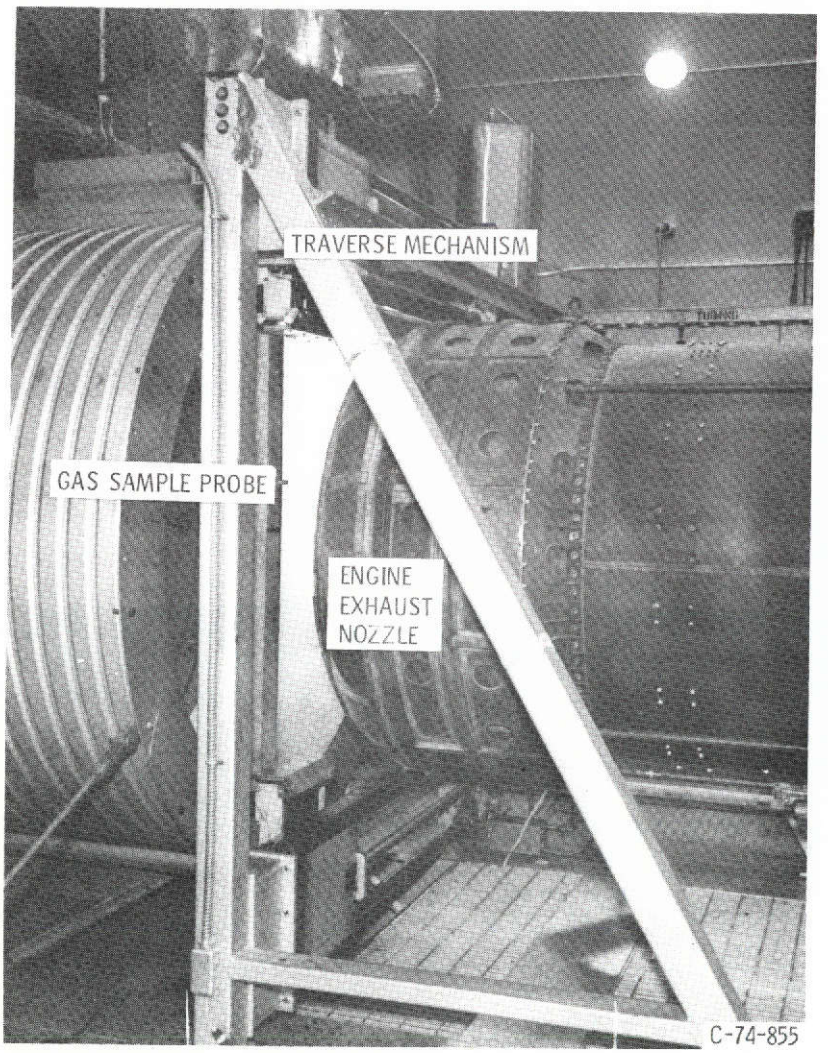

(a) PROBE AND TRAVERSING MECHANISM.

Figure 1. - Gas sample probe.

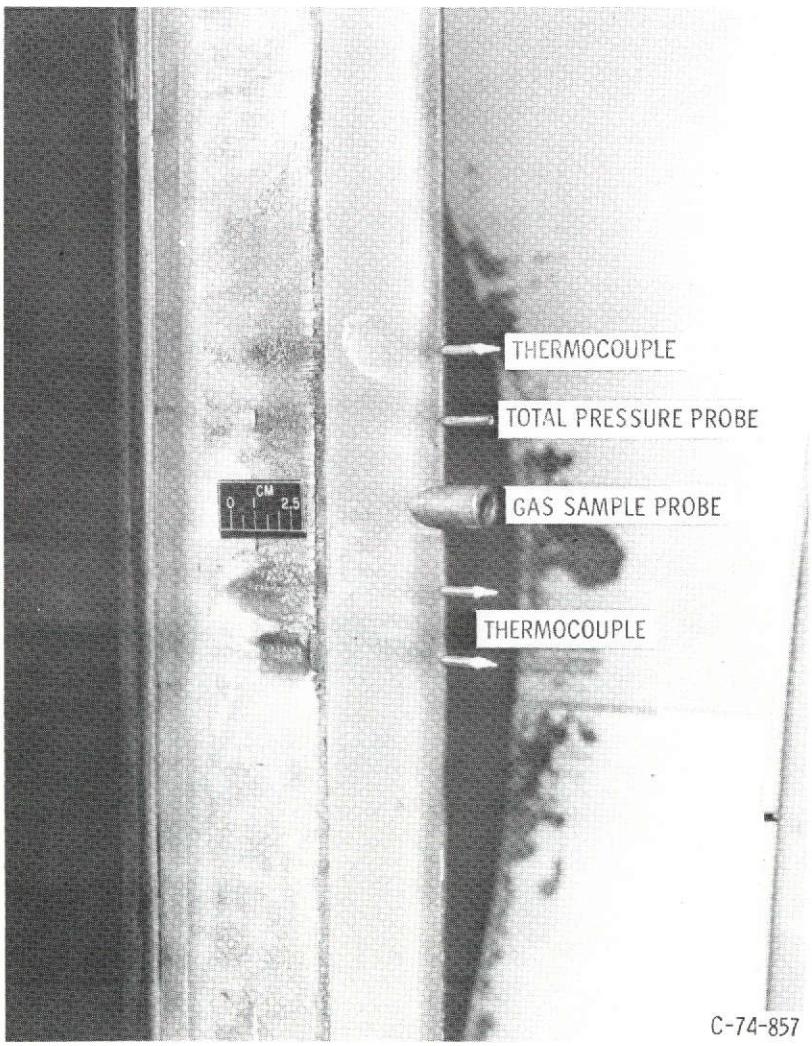

(b) DETAIL OF SENSOR AREA.

Figure 1. - Concluded.

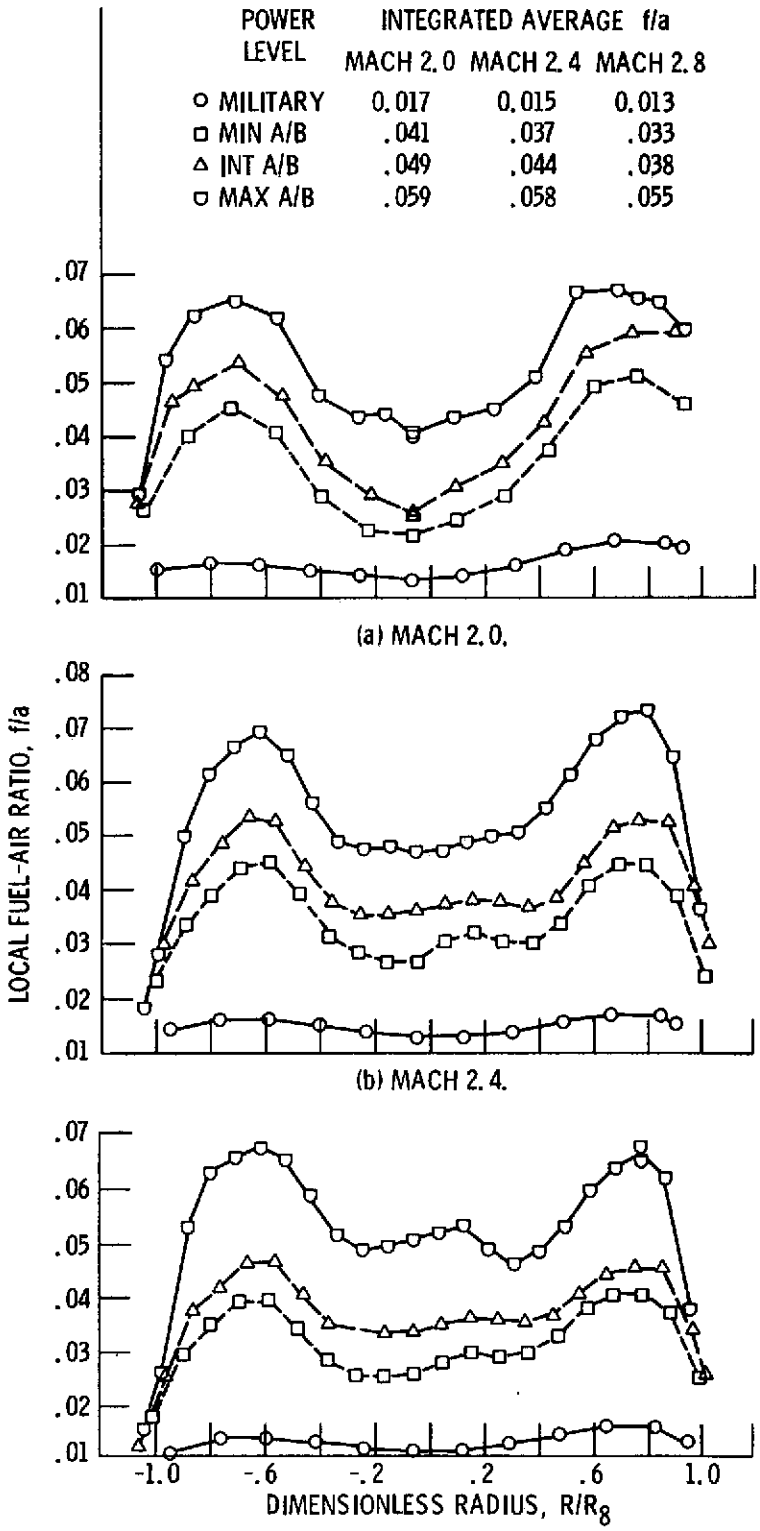

(a) MACH 2.0.

(b) MACH 2.4.

(c) MACH 2.8.

Figure 2. - Fuel-air ratio profiles.

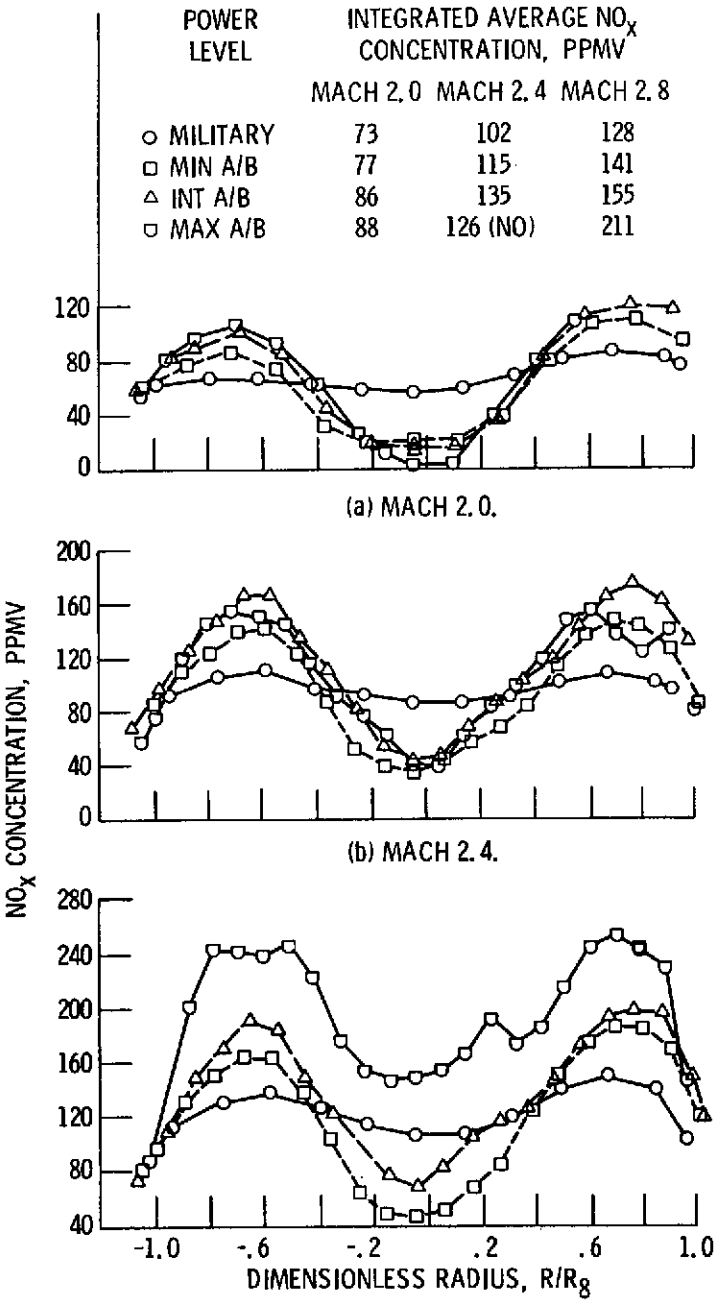

Figure 3. - Oxides of nitrogen concentration profiles.

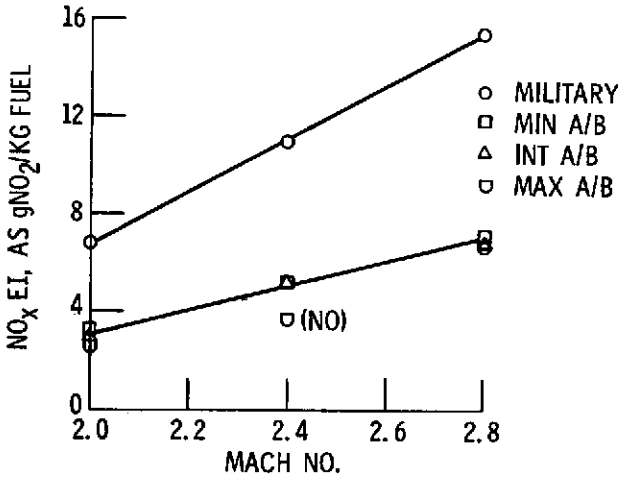

Figure 4. - Integrated average NO_X emission indices.

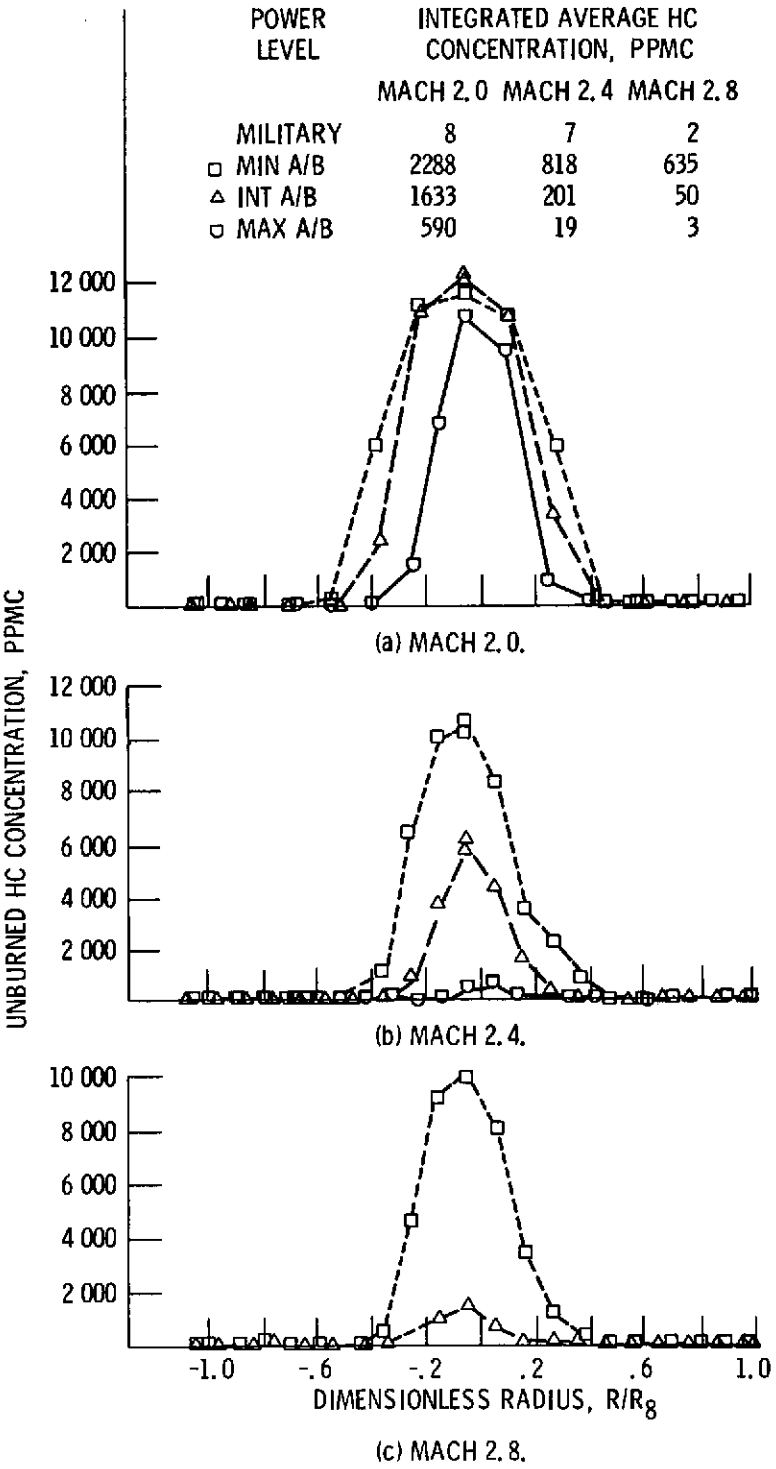

Figure 5. - Unburned hydrocarbons concentration profiles.

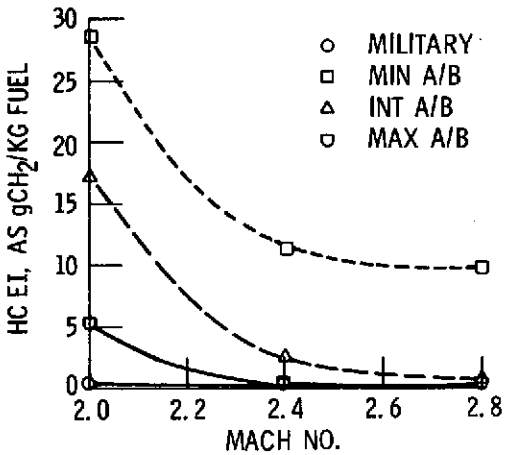

Figure 6. - Integrated average HC emission indices.

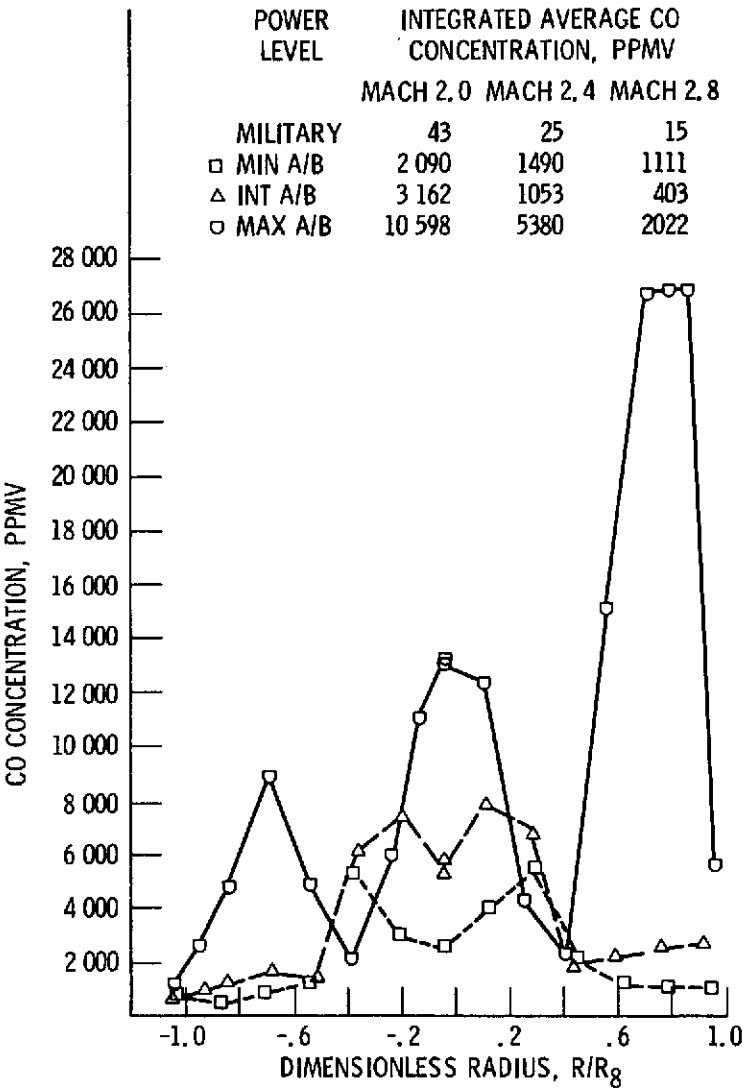

(a) MACH 2.0.

Figure 7. - Carbon monoxide concentration profiles.

POWER LEVEL	INTEGRATED AVERAGE CO CONCENTRATION, PPMV		
	MACH 2.0	MACH 2.4	MACH 2.8
MILITARY	43	25	15
□ MIN A/B	2 090	1490	1111
△ INT A/B	3 162	1053	403
○ MAX A/B	10 598	5380	2022

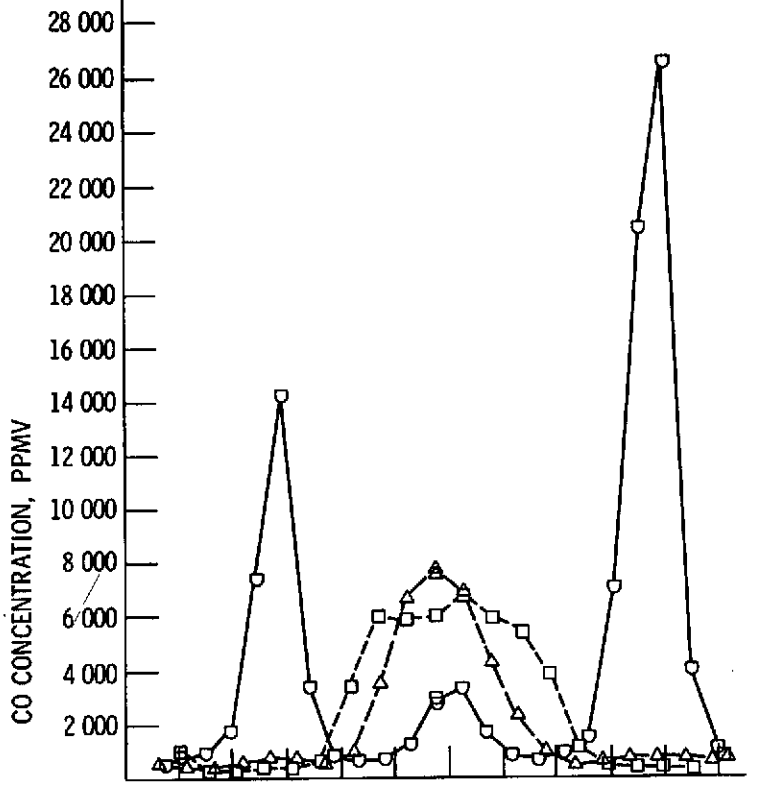

(b) MACH 2.4.

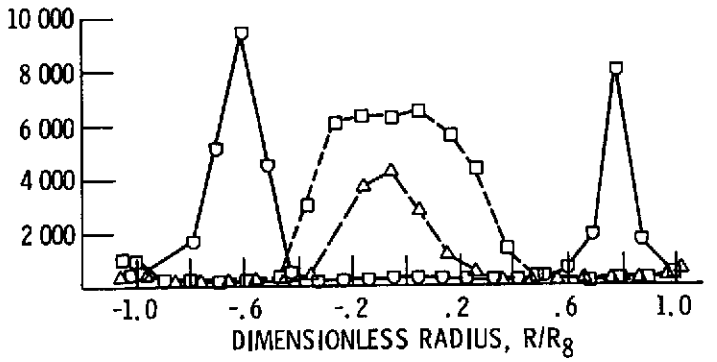

(c) MACH 2.8.

Figure 7. - Concluded.

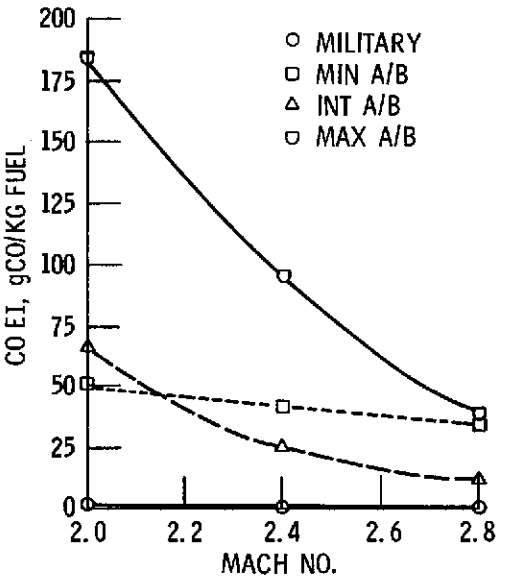

Figure 8. - Integrated average CO emission indices.

NASA-Lewis